SOME EXTENSIONS TO THE UNDERWEDGE-SURFACE ANGLE EFFECTS ON THE FLOWFIELD STRUCTURE OF A SHARP LEADING EDGE IN HYPERSONIC FLOW

Wilson F. N. Santos – wilson@lcp.inpe.br
Combustion and Propulsion Laboratory
National Institute for Space Research
Cachoeira Paulista, SP 12630-000

Abstract. *A computational investigation of the rarefied hypersonic flow over a flat plate with a sharp leading edge is presented. A Direct Simulation Monte Carlo (DSMC) method is applied to obtain a non-equilibrium state for the rarefied gas flow over the flat plate. Results for a flat plate with five different underwedge-surface angles and three wall temperatures are compared in order to assess the relative importance of the underwedge-surface angle and the wall temperature on the aerodynamic surface quantities. From these numerical simulations, interesting features were observed in the surface fluxes. It was found that small underwedge-surface angle has important effects on high Mach number leading edge flows.*

Keywords: *Hypersonic flow, Rarefied flow, DSMC, Sharp leading edge, Flat-plate.*

1. INTRODUCTION

Computer code validation for hypersonic low density flow often requires wind tunnel measurements in the flowfield and on the body surface with different physical quantities. Usually, a widely investigated configuration is the "infinitely thin" or "aerodynamically sharp" flat plate. Other common configurations, such as compression corners, forward or backward facing steps, also include flat plates as their upstream part. Nevertheless, the manufacturing and instrumentation processes of these models inevitable lead to flat plates of finite thickness, which have to be beveled in order to simulate "infinitely thin" or "aerodynamically sharp" models.

Experimental results with these models are compared with theoretical or numerical ones based on the assumption of a zero-thickness plate. As a result, it is desirable to estimate the largest underwedge-surface angle or bevel angle that allows meaningful comparison to be made. The reason for that is because all the experimental work has suffered with the problem of assessing the influence of the tip thickness t and underwedge-surface angle θ (see Fig. 1) on the measurements of the aerodynamic surface quantities, since it is not possible to investigate experimentally the special case of zero-tip thickness with or without zero-degree

underwedge-surface angle. In addition to that, experimental difficulty arises from the complication of installing pressure taps very close to the nose of the leading edge. In low-density flows, the true pressure on a surface can be significantly different from that measured in orifice cavities or pressure holes, because of the increase in the effect of molecule-surface collisions, the so-called orifice effect (Potter et al., 1966).

Numerous studies have been carried out in the past in order to investigate the influence of the leading edge shape and thickness on the flow over a given model. However, when a flat plate was considered, only few studies included a systematic variation of the underwedge-surface angle.

Hermina (1989) carried out DSMC calculation for comparison with available experimental data. However, results were presented for only one value of the leading-edge bevel angle. Thus, the above-mentioned problem remains open.

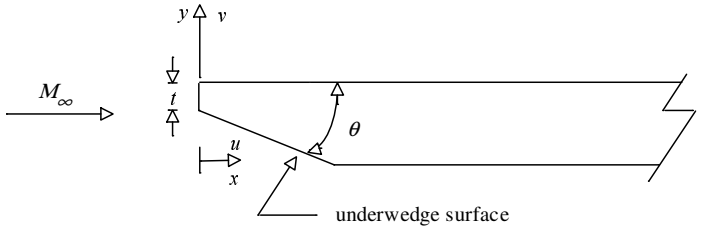

Figure 1: Drawing illustrating the leading edge shape.

In this scenario, Santos (2001) has investigated the sensitivity of the flowfield structure and the aerodynamic surface quantities to leading-edge thickness variations for a flat plate in a low-density hypersonic flow. The range of Knudsen number, based on the tip thickness t, covered from the transition flow regime to the free molecular flow regime. Nevertheless, the effect of the underwedge-surface angle θ was not investigated.

Santos (2007) extended further the previous analysis (Santos, 2001) by investigating closer the underwedge-surface angle effects. In this fashion, a parametric study was performed on a flat plate with zero-tip thickness in order to assess the impact on the primary properties upstream the nose of the leading edge due to variations on the underwedge-surface angle.

In an effort to obtain further insight into the nature of the flowfield structure of sharp leading edge under hypersonic transition flow conditions, the primary interest in the present account is to extend further the previous analysis (Santos, 2001, and 2007) by investigating closer the underwedge-surface angle combined with the wall temperature effects. In this manner, a parametric study is performed on a flat plate in order to assess the impact on the aerodynamic surface quantities due to variations on the bevel angle and on the wall temperature.

2. COMPUTATIONAL METHOD

A particle simulation method that has proved to be very effective as an engineering tool for the prediction of rarefied flow is the Direct Simulation Monte Carlo method (Bird, 1994). DSMC method employs thousands simulated particles to reproduce the behavior of a far large number of particles in the flow. The simulated particles are allowed to move and collide, while the computer stores their position coordinates, velocities and other physical properties such as internal energy. A computational grid is used to represent the simulated region. Statistical techniques are employed to reproduce the correct macroscopic behavior.

Collisions in the present DSMC code are modeled by using the variable hard sphere (VHS) molecular model (Bird, 1981) and the no time counter (NTC) collision sampling technique (Bird, 1989). Repartition energy among internal and translational modes is controlled by the Borgnakke-Larsen statistical model (Borgnakke and Larsen, 1975). Simulations are performed using a non-reacting gas model consisting of N_2 and O_2. Energy exchanges between the translation and internal modes, rotation and vibration, are considered.

Relaxation collision numbers of 5 and 50 were used for the calculations of rotation and vibration, respectively.

For the numerical treatment of the problem, the flowfield around the leading edge is divided into an arbitrary number of regions, which are subdivided into computational cells. Cells are further subdivided into subcells, two subcells/cell in each coordinate direction. The cell provides a convenient reference for the sampling of the macroscopic gas properties, while the collision partners are selected from the same subcell for the establishment of the collision rate. The computational domain used for the calculation is made large enough so that body disturbances do not reach the upstream and side boundaries, where freestream conditions are specified.

3. COMPUTATIONAL CONDITIONS

The freestream and flow conditions used in the present calculations are those given by Santos (2007) and summarized in Table 1. The gas properties (Bird, 1994) employed in the simulations are shown in Table 2. Referring to Tables 1 and 2, T_∞, p_∞, ρ_∞, n_∞, μ_∞, and λ_∞ stand respectively for temperature, pressure, density, number density, viscosity and mean free path, and X, m, d and ω account respectively for mole fraction, molecular mass, molecular diameter and viscosity index.

Table 1: Freestream Conditions

T_∞ (K)	p_∞ (N/m^2)	ρ_∞ (kg/m^3)	n_∞ (m^{-3})	μ_∞ (Ns/m^2)	λ_∞ (m)	U_∞ (m/s)
220.0	5.582	8.753×10^{-5}	1.8209×10^{21}	1.455×10^{-5}	9.03×10^{-4}	3560

Table 2: Gas Properties

	X	m (kg)	d (m)	ω
O_2	0.237	5.312×10^{-26}	4.01×10^{-10}	0.77
N_2	0.763	4.65×10^{-26}	4.11×10^{-10}	0.74

The freestream velocity U_∞, assumed to be a constant at 3.56 km/s, corresponds to freestream Mach number M_∞ of 12. The Reynolds number per unit of meter is $Re_\infty = 21416.3$, also based on conditions in the undisturbed stream.

In the previous study, Santos (2001), the reference flow scale was defined as being the tip thickness t of the flat plate. The tip thickness investigated was t/λ_∞ of 0.2, 0.1, 0.05, 0.025, 0.02, 0.0125 and 0.01, where λ_∞ was the freestream mean free path. Therefore, the overall Knudsen number Kn_t, defined as the ratio of the freestream mean free path λ_∞ to the tip thickness t, corresponded to 5, 10, 20, 40, 50, 80 and 100, respectively.

In Santos (2007), the underwedge-angle effects were investigated independently for five distinct numerical values of underwedge-surface angle θ of 5, 10, 15, 20 and 25 degrees with zero-thickness flat plate, which corresponded to Kn_t of infinity.

In order to simulate the wall temperature effect, in the present account the DSMC calculations were performed independently for three distinct numerical values of wall temperature, i.e., T_w of 440 K, 880 K and 1760 K. These values correspond to 2, 4 and 8 times the freestream temperature, respectively.

4. COMPUTATIONAL RESULTS AND DISCUSSION

The purpose of this section is to discuss and to compare differences in the aerodynamic properties due to variations on the underwedge-surface angle and on the wall temperature. The surface properties of particular interest in the present account are number flux, heat flux, and wall pressure.

The number flux N is calculated by sampling the molecules impinging on the surface by unit time and unit area. The sensitivity of the number flux to the upper- and lower-body surfaces due to variations on the wall temperature is illustrated in Figs. 2 and 3, respectively, parameterized by the underwedge-surface angle θ. In this set of figures, the dimensionless number flux N_f stands for the number flux N normalized by $n_\infty U_\infty$, where n_∞ is the freestream number density. Furthermore, S is the length s along the upper- or lower-body surfaces, measured from the stagnation point, normalized by the freestream mean free path λ_∞. For comparison purpose, the dimensionless number flux to the upper surface by considering free molecular (FM) flow (Bird, 1994) is shown. In addition, the special case of zero-degree underwedge-surface angle was included in this set of figures. In this fashion, the particular case of zero-degree angle represents a zero-tip thickness flat plate. As was mentioned earlier, this special case can not be investigated experimentally.

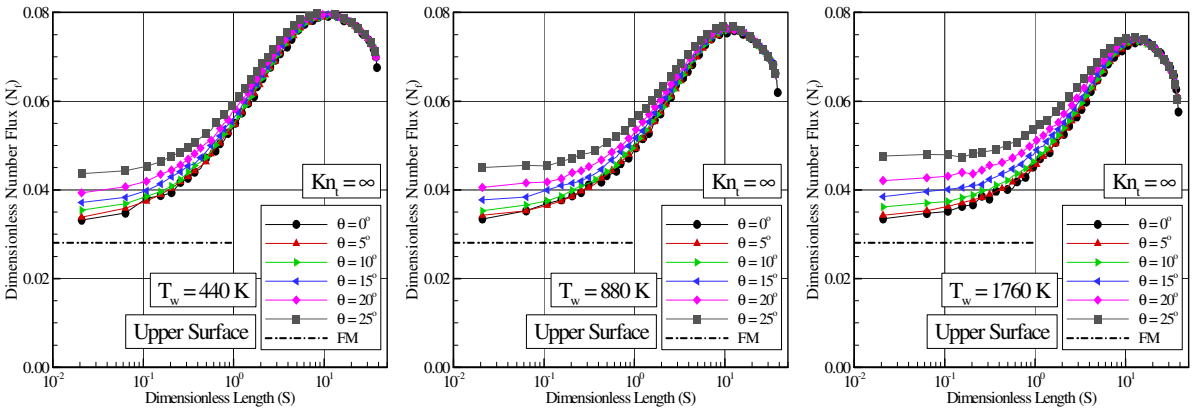

Figure 2: Dimensionless number flux N_f along the upper-body surface as a function of the underwedge-surface angle θ and wall temperature T_w of (a) 440 K, (b) 880 K and (c) 1760 K.

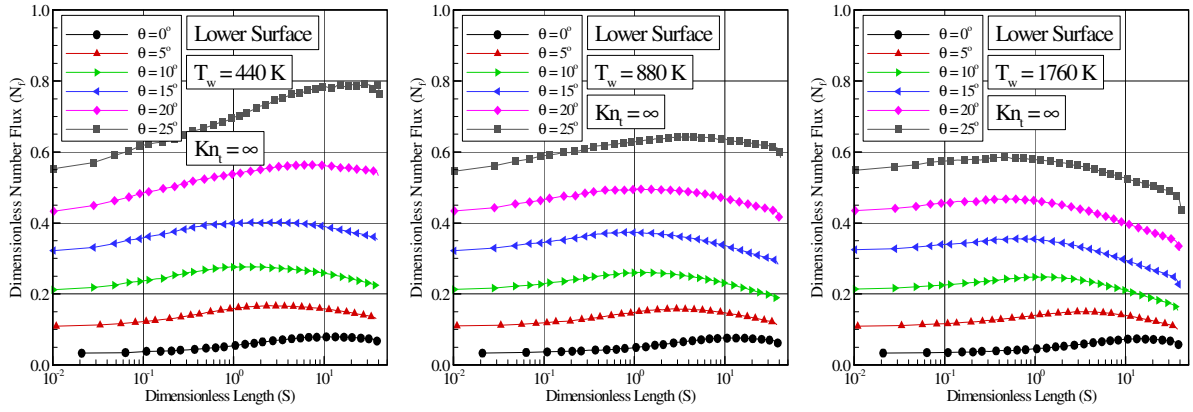

Figure 3: Dimensionless number flux N_f along the lower-body surface as a function of the underwedge-surface angle θ and wall temperature T_w of (a) 440 K, (b) 880 K and (c) 1760 K.

Referring to Figs. 2 and 3, it is seen that the number flux to the upper surface is low at the leading edge and increases substantially up to a maximum value located at about $10\lambda_\infty$ downstream along the upper surface of the plate for the zero-degree underwedge angle case. With the underwedge-angle rise, the number flux increases not only on the lower-body surface but also on the upper-body surface. Along the lower plate surface, the number flux increases dramatically along the whole plate, whereas a significant number flux increase is observed up to a distance of $10\lambda_\infty$ downstream along the upper part of the plate for some underwedge angles. This increase in the dimensionless number flux along the upper surface of the plate with increasing the underwedge angle may be related to the collisions of two groups of molecules; the molecules reflecting from the plate surface, at the vicinity of the leading edge, and the molecules oncoming from the freestream, as mentioned earlier. The molecules that are reflected from the body surface, which have a lower kinetic energy interact with the oncoming freestream molecules, which have a higher kinetic energy. Thus, the surface-reflected molecules recollide with the body surface, which produce an increase in the dimensionless number flux in this region. This effect is less pronounced with increasing the body-surface temperature. By increasing the wall temperature, the molecules are reflected with more energy.

The heat transfer coefficient C_h is defined as being,

$$C_h = \frac{q_w}{\frac{1}{2}\rho_\infty U_\infty^3} \tag{1}$$

where where ρ_∞ is the freestream density, and the heat flux q_w to the body surface is calculated by the net energy fluxes of the molecules impinging on the surface. A flux is regarded as being positive if it is directed toward the surface. The heat flux q_w is related to the sum of the translational, rotational and vibrational energies of both incident and reflected molecules as defined by,

$$q_w = q_i + q_r = \sum_{j=1}^{N} \left\{ \left[\frac{1}{2} m_j v_j^2 + e_{Rj} + e_{Vj} \right]_i + \left[\frac{1}{2} m_j v_j^2 + e_{Rj} + e_{Vj} \right]_r \right\} \tag{2}$$

where N is the number of molecules colliding with the surface by unit time and unit area, m is the mass of the molecules, v is the velocity of the molecules, e_R and e_V stand for the rotational and vibrational energies, respectively. Subscripts i and r refer to incident and reflected molecules.

Effects on the heat transfer coefficient C_h due to changes on the wall temperature and on the underwedge-surface angle θ are displayed in Figs. 4 and 5 for upper- and lower-body surfaces, respectively. According to this set of plots, it is clearly seen that the underwedge-surface angle affects the heat transfer coefficient distribution on the upper and lower surfaces of the leading edge. It is also observed that the heat transfer coefficient C_h approaches the free molecular limit from above. This behavior is directly related to the number flux rise discussed earlier. It is noteworthy that the free molecular limit on the lower surface (not shown) depends on the underwedge-surface angle θ.

According to this set of figures, the behavior of the heat transfer coefficient C_h with wall temperature rise is as expected in the sense that the heat transfer coefficient decreases with increasing wall temperature. The heat flux to the body surface was defined in terms of the incident and reflected flow properties, Eq. (2), and based upon the gas-surface interaction model of fully accommodated, complete diffuse re-emission. The diffuse model assumes that the molecules are reflected equally in all directions, quite independently of their incident

speed and direction. Due to the diffuse reflection model, the reflected velocity of the molecules impinging on the body surface is obtained from a Maxwellian distribution that takes into account for the temperature of the body surface. In this fashion, according to Eq.(2), not only the number of molecules impinging on the surface but also the wall temperature plays a important role on the reflected contribution to the net heat flux to the body surface. Consequently, the reflected contribution of the molecules increases with increasing the wall temperature, and the net heat flux or the heat transfer coefficient decreases with wall temperature rise.

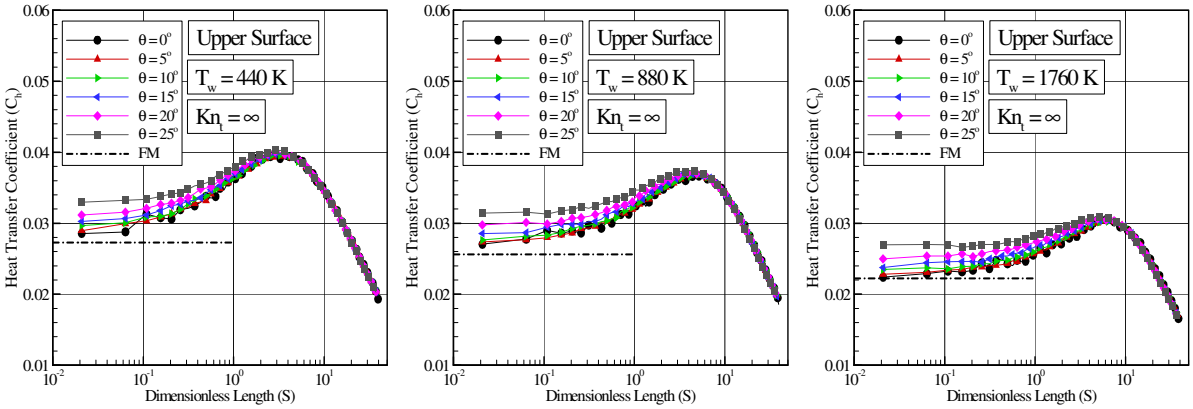

Figure 4: Heat transfer coefficient C_h along the upper-body surface as a function of the underwedge-surface angle θ and wall temperature T_w of (a) 440 K, (b) 880 K and (c) 1760 K.

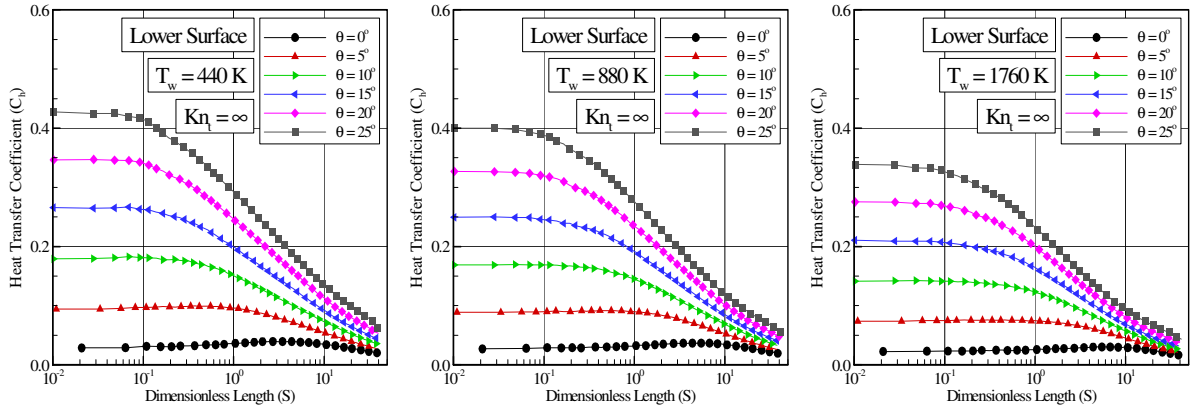

Figure 5: Heat transfer coefficient C_h along the lower-body surface as a function of the underwedge-surface angle θ and wall temperature T_w of (a) 440 K, (b) 880 K and (c) 1760 K.

The pressure coefficient C_p is defined as being,

$$C_p = \frac{p_w - p_\infty}{\frac{1}{2}\rho_\infty U_\infty^2} \tag{3}$$

where p_w is the pressure acting on the body surface and p_∞ is the freestream pressure.

The pressure p_w on the body surface is calculated by the sum of the normal momentum fluxes of both incident and reflected molecules at each time step by the following expression,

$$p_w = p_i + p_r = \sum_{j=1}^{N} \left\{ \left[m_j v_{\eta j} \right]_i + \left[m_j v_{\eta j} \right]_r \right\} \tag{4}$$

where v_η is the normal velocity component of the molecules.

The impact on the pressure coefficient C_p due to changes on the wall temperature and on the underwedge-surface angle θ is demonstrated in Figs. 6 and 7 for upper- and lower-body surfaces, respectively. According to this group of plots, it is noted that the pressure coefficient follows the same trend as that presented by the number flux in that it is low at the leading edge and increases substantially up to a maximum value located at about $10\lambda_\infty$ downstream along the upper surface of the plate. It is clearly noticed that the pressure coefficient is sensitive to the underwedge-surface angle and to the wall temperature in the sense that it increases with increasing the underwedge-surface angle and the wall temperature. As an illustrative example, for wall temperature of 440 K and 5-, 15-, and 25-degree underwedge angles, C_p is, respectively, 8.2%, 50.8% and 135.1% larger than the pressure coefficient C_p for the special case of zero-degree underwedge angle. On the other hand, the pressure coefficient C_p for wall temperature of 1760 K and θ of 0, 5, 15 and 25 degrees is 133.3%, 132.7%, 115.5% and 103.6% larger than that for wall temperature of 440 K, respectively.

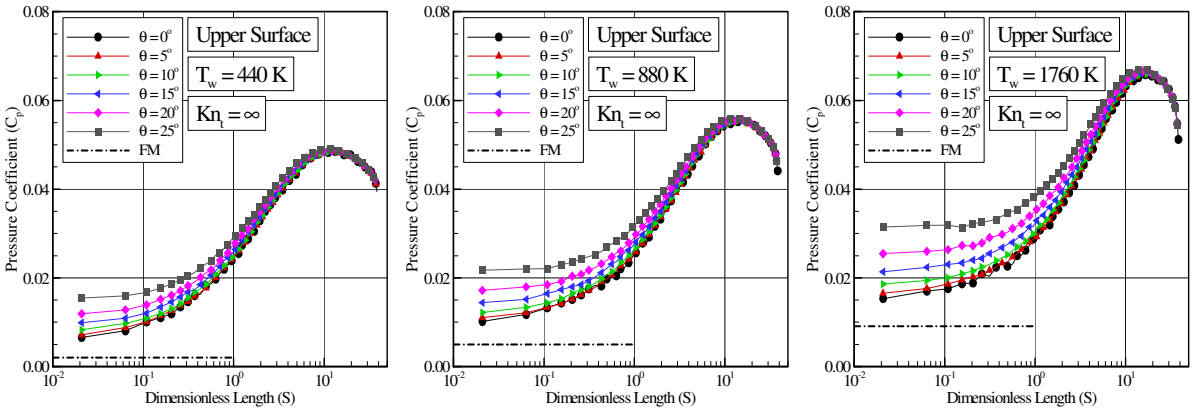

Figure 6: Pressure coefficient C_h along the upper-body surface as a function of the underwedge-surface angle θ and wall temperature T_w of (a) 440 K, (b) 880 K and (c) 1760 K.

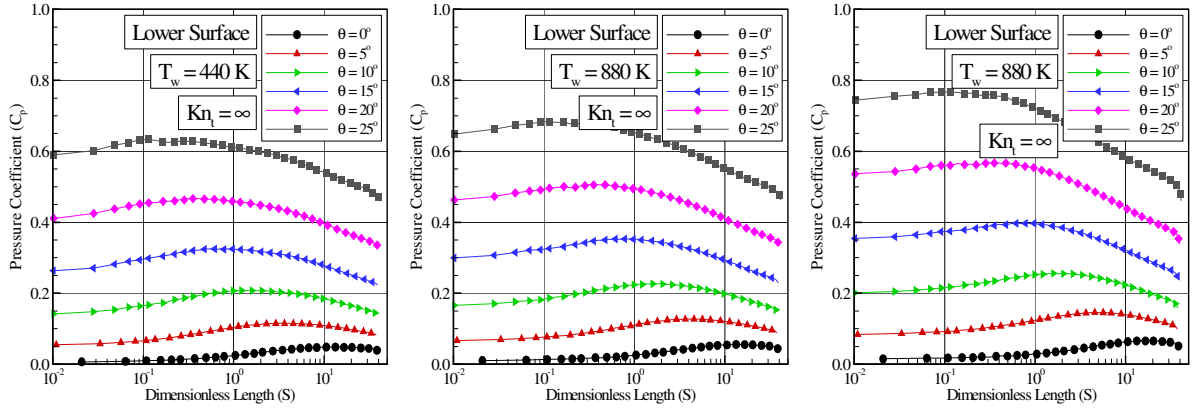

Figure 7: Pressure coefficient C_h along the lower-body surface as a function of the underwedge-surface angle θ and wall temperature T_w of (a) 440 K, (b) 880 K and (c) 1760 K.

Based on the behavior of the aerodynamic surface quantities along the upper-body surface illustrated in Figs. 2, 4, and 6, it is firmly established that the flowfield below the centerline affects the surface quantities on the upper surface. Therefore, at this point it is worth taking a closer look at the flowfield structure around the leading edges.

In order to emphasize interesting features in the flowfield structure around the sharp leading edges, the streamline traces at the vicinity of the leading edges are depicted in Figs. 8(a-c) for underwedge-surface angle θ of 5, 15 and 25 degrees, respectively, and wall temperature of 880 K. In this set of diagrams, X and Y stand, respectively, by the length x and the height y normalized by the freestream mean free path. Also, it should be remarked that different scales are used in the x- and y-axis.

According to Figs. 8(a-c), it is recognized that the streamlines along to and upper to the centerline are displaced upward by increasing the underwedge-surface angle θ. In addition to that, the streamlines located immediately below to the centerline pass around to the upper surface of the leading edges. A similar behavior is observed for the other cases (not shown), i.e., wall temperature of 440 K and 1760 K.

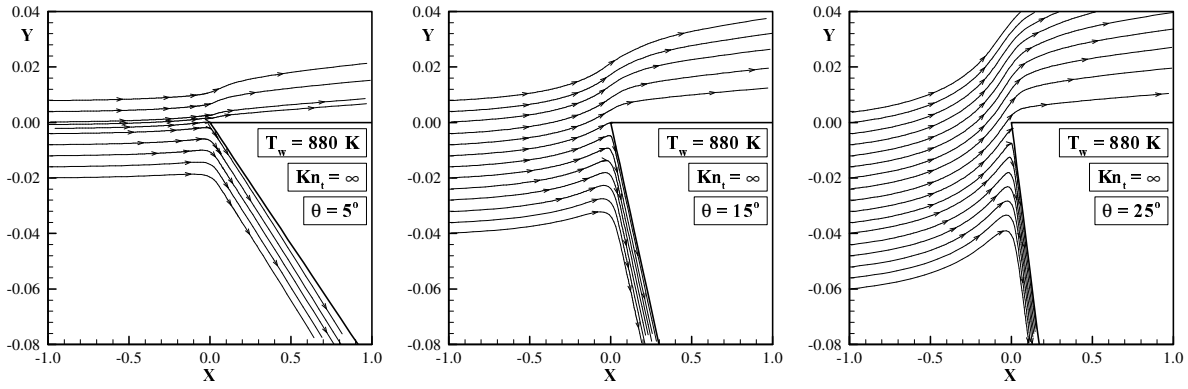

Figure 8: Streamline traces at the vicinity of the leading edges for underwedge-surface angle θ of (a) 5, (b) 15 and (c) 25 degrees and wall temperature of 880 K.

For the time being, it becomes instructive to quantify the contribution of the flowfield, which comes from below the centerline, to the aerodynamic surface quantities on the upper-body surface. A convenient way of doing this is to identify the molecules in an appropriate way. In this manner, freestream molecules entering the computational domain above the centerline of the leading edges were identified (flagged) by type I, and those freestream molecules entering below the centerline were identified as type II. As a result of this procedure, the number flux, the heat flux and the wall pressure may be expressed by the contribution of the two types of the molecules.

The distribution of the number flux along the upper- and lower-body surfaces is displayed in Figs. 9 and 10, respectively, as a function of the underwedge-surface angle and of the wall temperature.

According to this set of plots, it is quite apparent that not only molecules type II (originated from below the centerline) affects the number flux distribution on the upper-body surface but also molecules type I (originated from above the centerline) contributes to the number flux on the lower-body surface. It is very encouraging to observe that the contribution of the molecules type II to the number flux to the upper-body surface increases with the underwedge-surface angle for the range investigated. Nevertheless, no appreciable effect is observed with the wall temperature rise.

It should be mentioned in this context that the number flux is the number of molecules

impinging on the surface by unit time and unit area. As a result, the heat flux and the wall pressure depend on this number as shown in Eqs. (2) and (4). Consequently, molecules type I and II will affect the heat flux and the wall pressure in a similar way.

These results are extremely important in the sense that they indicate that, with the size of the models, for instance flat plate, being tested in hypersonic tunnels, significant effects on the flowfield properties as well as on the aerodynamic surface quantities, due to leading-edge thickness and underwedge-surface angle are possible even with models whose leading edges are generally considered as being either "infinitely thin" or "aerodynamically sharp".

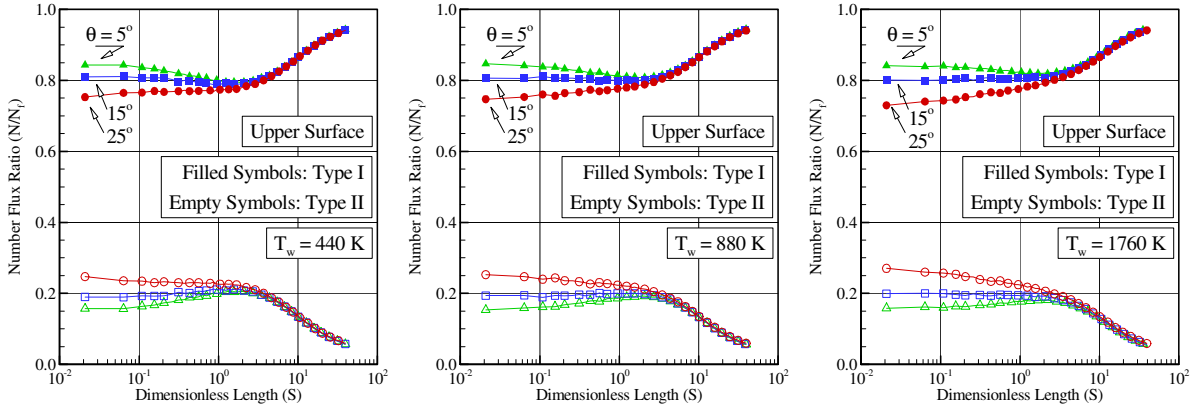

Figure 9: Number flux ratio (N/N_f) along the upper-body surface as a function of the underwedge-surface angle θ and wall temperature T_w of (a) 440 K, (b) 880 K and (c) 1760 K.

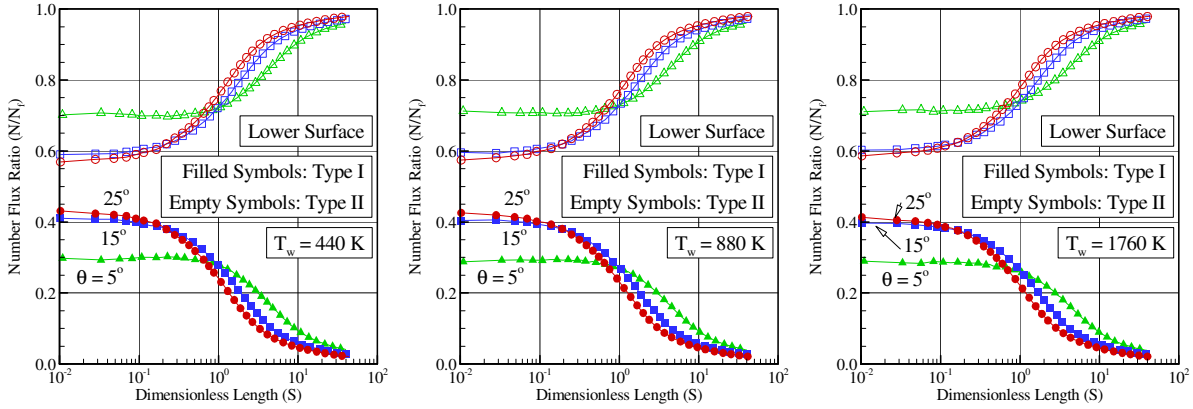

Figure 10: Number flux ratio (N/N_f) along the lower-body surface as a function of the underwedge-surface angle θ and wall temperature T_w of (a) 440 K, (b) 880 K and (c) 1760 K.

5. CONCLUDING REMARKS

This study applies the Direct Simulation Monte Carlo (DSMC) method to assess the impact on the aerodynamic surface quantities due to variations on the wall temperature and on the underwedge-surface angle of flat plates. The calculations provided information concerning the surface quantities in coefficient form defined by number flux, heat transfer, and pressure acting on the body surface for the idealized situation of two-dimensional hypersonic rarefied flow.

The simulations pointed out that the aerodynamic surface quantities increased on the upper surface of the flat plate with the underwedge-surface angle rise. It was found that pressure was more affected than the heat flux with increasing the underwedge-surface angle.

The analysis showed that the wall temperature rise affected the aerodynamic surface quantities in a different way. The pressure coefficient increased along the upper-body surface. In contrast, the heat flux to the body surface decreased as would be expected.

REFERENCES

Bird, G. A., 1981, Monte Carlo simulation in an engineering context, in Sam S. Fisher, ed., *Progress in Astronautics and Aeronautics: Rarefied gas Dynamics*, vol. 74, part I, pp. 239-255, AIAA New York.

Bird, G. A., 1989, Perception of numerical method in rarefied gasdynamics, in E. P. Muntz, and D. P. Weaver and D. H. Capbell, eds., *Rarefied gas Dynamics: Theoretical and Computational Techniques*, Progress in Astronautics and Aeronautics, AIAA, New York, vol. 118, pp. 374-395.

Bird, G. A., 1994, *Molecular Gas Dynamics and the Direct Simulation of Gas Flows*, Oxford University Press, Oxford, England, UK.

Borgnakke, C. & Larsen, P. S., 1975, Statistical collision model for Monte Carlo simulation of polyatomic gas mixture, *Journal of Computational Physics*, vol. 18, n. 4, pp. 405-420.

Potter, J. L., Kinslow, M. & Boylan, D. E., 1966, An influence of the orifice on measured pressures in rarefied flow, in J. H. de Leeuw, ed., *Rarefied Gas Dynamics*, Academic Press, New York, vol. II, pp. 175-194.

Hermina, W. L., 1989, Monte Carlo simulation of rarefied flow along a flat plate, *Journal Thermophysics and Heat Transfer*, vol. 3, n. 1, pp. 7-12.

Santos, W. F. N., 2001, Rarefied hypersonic flow past the sharp/blunt leading edge of a flat plate, in *2nd International Conference on Computational Heat and Mass Transfer*, Rio de Janeiro, RJ, Brazil.

Santos, W. F. N., 2007, The underwedge-surface angle effects on the flowfield structure of a sharp leading edge in hypersonic flow, in *X Encontro de Modelagem Computacional*, 21-23 november, Nova Friburgo, RJ.